Underwater Image Dehazing via Red-Channel Recovery

Elif Duygu Petenkaya
Izmir University of Economics
Izmir, Turkey

Ozge Basak Lacin
Izmir University of Economics
Izmir, Turkey

Omer Faruk Kara
Izmir University of Economics
Izmir, Turkey

Mehmet Turkan
Izmir University of Economics
Izmir, Turkey

Abstract—Due to light scattering and absorption while traveling through water, underwater images become hazy and loose critical information resulting in poor contrast and weak color performance. Hence, it is difficult to see the difference between foreground colors and items, and to differentiate the background in these images. To solve these issues, this study proposes a novel technique for single underwater image enhancement which relies on the recovery of the lost red-channel via a weighted multi-scale fusion. Firstly, three color balance algorithms are applied to the input image to gain more information about the scene. Then, five weight maps are extracted from these balanced versions of the input image to emphasize fine-details. Finally, the enhanced output is obtained with the new red-channel, white balanced green and blue channels followed by gamma correction to maintain contrast of the image. The developed method produces higher-quality underwater images that can be evaluated qualitatively and quantitatively when compared to state-of-the-art approaches.

Index Terms—underwater image dehazing, underwater image enhancement, red-channel recovery, image enhancement

I. INTRODUCTION

The physical features of the subsea environment make underwater image processing very difficult. Absorption and scattering weaken the collected underwater images in many circumstances. Since the light is dynamically retained because it passes through the water, submerged images are characterized by their low visibility, poor colors and strong haze. As a result, a compelling strategy for enhancing underwater images for both visualization and analysis is significant, and so craved [1].

In an underwater environment, light can be diverted by particles that are the same estimate as the light wavelengths or particles that have a diverse refraction list than the water [2]. There are several studies proposed in literature to improve underwater image quality. In the milestone work of He *et al.* [3], the proposed method presents a prior based on the dark channel information to reduce the haze from a single image. The developed method succeeds in estimating the thickness of the haze and recovers a haze-free output by combining the prior with the haze model. In the other study developed by Yadav *et al.* [4], a contrast limited adaptive histogram equalization (CLAHE) is employed to improve the foggy vision. In this approach, the "distribution" parameter is utilized to specify the form of the histogram, which produces higher-quality outcomes than adaptive histogram equalization. Huang *et al.* [5] propose an effective shallow-water image enhancement method via relative global histogram stretching (RGHS) with adaptive parameters. This method contains of two components as contrast correction and color correction. In another study by Iqbal *et al.* [6], an unsupervised color correction method (UCM) is developed for underwater image enhancement. It is based on color balancing and contrast correction in RGB and HSI color spaces. Ancuti *et al.* [7], [8] build single image dehazing algorithms by means of the weighted (multi-scale) fusion principle using color compensation and white balancing, which lead to less noise, better exposedness in the dark regions, corrected contrast, fine-details and sharp edges in the output images.

There exist also deep learning algorithms for the underwater image enhancement problem. However, traditional architectures are mostly successful for synthetic images but less effective for real-world scenes. In the study of Park *et al.* [9], a novel approach via cycle-consistent generative adversarial networks (CycleGAN) with a pair of content discriminators is proposed to effectively enhance underwater images. In another study, Li *et al.* [10] propose a fusion adversarial network (FGAN) to dehaze underwater images. This network successfully corrects color cast issues and low contrast problems with faster testing time and less parameters.

To this end, this study proposes a novel underwater image enhancement method to achieve better dehazed and more realistic output images in comparison to state-of-the-art approaches in literature. The developed method builds upon principal component analysis (PCA), well-exposedness [11], [12], saliency [13], brightness and Laplacian contrast feature maps through a weighted multi-scale fusion in order to successfully recover the lost red-channel back. The designed method is compared with well-known underwater image enhancement algorithms and it shows strong outputs both statistically and visually.

This paper is organized as follows. Section II details the proposed underwater image enhancement method. Section III reports the experimental setup and discusses the results in comparison to competing algorithms in literature. Finally,
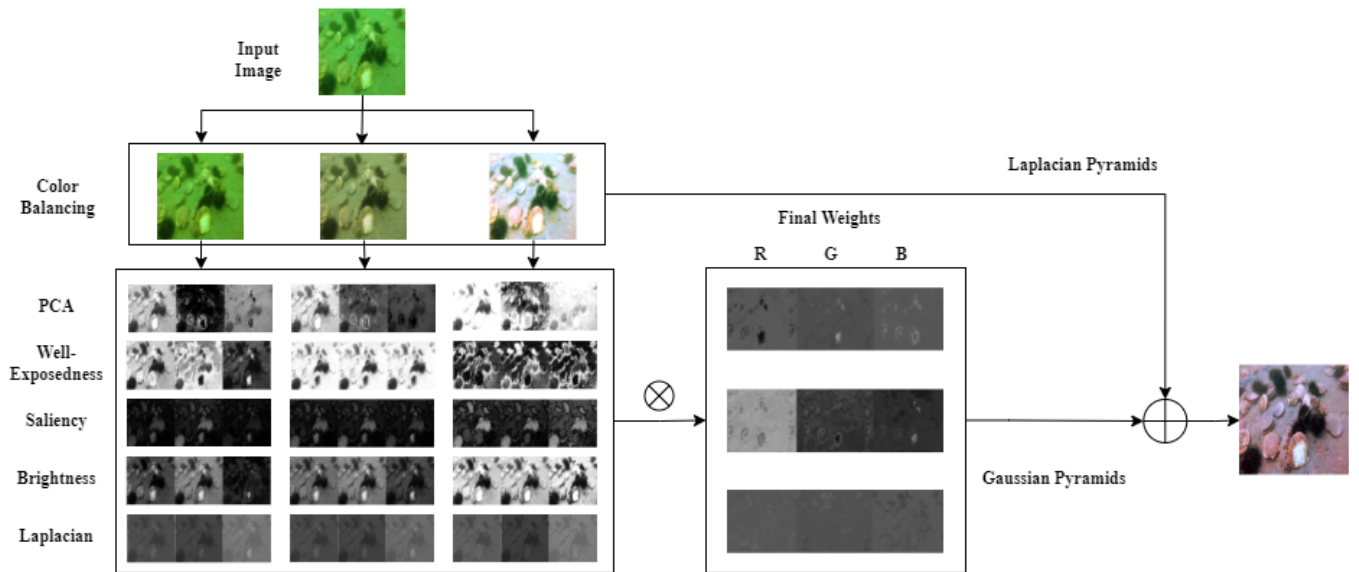
Fig. 1. Flowchart of the proposed method.

Sec. IV concludes this paper with a brief conclusion.

II. PROPOSED DEHAZING METHOD

A complete flowchart of the developed image enhancement method is given in Fig. 1. At first, the input hazy image is color balanced with three different algorithms (i.e., color compensation [14], Gray World [15], white balance [16]) to extract more information from the scene. At second, five different weight maps (i.e., PCA, well-exposedness, saliency, brightness, Laplacian contrast) are featured from these balanced versions of the input image to highlight the details. These features are then combined to form refined weights to be used in the final multi-scale fusion step. After the fusion stage, the enhanced output is obtained with the new red-channel; and simply white-balanced blue and green channels of the input image followed by a gamma correction as post-processing. The remaining part of this section describes all details of the proposed method.

A. Color Balance Algorithms

Color Compensation. An accurate identification of the channel to be corrected is almost impossible due to low contrast and under exposure nature of underwater images. With the long-wavelength attenuation phenomena, the particular focus is on the red-channel compensation approach of Kumar and Bhandari [14] given in Eqn. (1) as

$$I'_R(x) = I_R(x) + \alpha(\bar{I}_G - \bar{I}_R)(1 - I_R(x))I_G(x) \quad (1)$$

where $I'_R(x)$ represents the intensity of compensated red-channel at pixel location x, $I_R(x)$ and $I_G(x)$ denotes the intensity of the red and green channels of the original image at x, $\bar{I}_R$ and $\bar{I}_G$ are the average values of these channels, respectively. All channel intensity values are normalized to the range $[0, 1]$ and the illumination parameter α varies in

$[0, 1]$. To avoid possible overcompensation, the red-channel compensation is applied to locations with low values of this channel through green channel only.

Gray World. Gray World is a conventional color constancy method that assumes the average reflectance of surfaces in the world is achromatic [15]. The algorithm is described by Eqn. (2) as

$$I'_*(x) = \frac{I_*(x)}{\bar{I}_*} gray \quad (2)$$

where $I_*(x)$ represents one of the three color channels R, G and B at pixel location x, $I'_*(x)$ is the color corrected version of the corresponding channels at x, $\bar{I}_*$ is the average intensity value of I_* and $gray$ denotes a predefined parameter towards which the intensity values of each channel are updated. The value of $gray$ varies depending on the application and it is set to 195 in this study.

White Balance. White balance seeks to compensate the color cast arising from selective absorption of colors with the depth of water. In this study, the white balance method first sums all color channels, finds the brightest pixel and its location, and then applies color correction using scene illumination, i.e., Max RGB [16].

B. Weight Extraction

PCA. PCA feature maps [12] are extracted for each color channel of each color balanced version of the input image. Aligned with the theory of the PCA algorithm, it aims at giving more weight to the dominant pixels of an image.

Let I_R, I_G and I_B be the color channels of sizes $r \times c$ pixels. These three channels are first vectorized and then put into columns of an $rc \times 3$ data matrix (rc observations with 3 variables) to calculate observation scores of PCA.

Consequently, each score vector is linearly normalized to the range $[0, 1]$, and reshaped back to an $r \times c$ weight matrix P_{I_*}, where I_* represents one of the three color channels R, G and B.

Well-exposedness. The feature of well-exposedness determines how effectively a pixel is exposed [11], [12]. It aims at highlighting intensities which are not so close to 0 (dark regions) or 1 (saturated regions), hence it favors pixels in well-exposed regions with intensities close to 0.5. All channel intensity values are assumed to be normalized to the range $[0, 1]$.

For a given color balanced image, this feature is obtained for each color channel I_R, I_G and I_B using a Gaussian curve given in Eqn. (3) as

$$E_{I_*} = exp\left(-\frac{(I_* - 0.5)^2}{2\sigma^2}\right) \tag{3}$$

where E_{I_*} denotes the well-exposedness map of the color channel I_* and σ is set to 0.2.

Saliency. Several saliency modeling techniques have been presented in literature to simulate the human visual system, hence to highlight important regions and improve the visual quality of images [12]. Saliency features are utilized in this study to assign larger weights to pixels that are more salient to human observers. The DCT based technique introduced by Hou *et al.* [13] is adopted, resulting in S_{I_*} saliency maps for each color channel R, G and B of each color balanced version of the input image.

Brightness. The brightness of an image is determined by saturation, which is a significant impact element [17]. High brightness always aids in the creation of more vivid colors.

In this study, brightness of a pixel is simply measured by its absolute deviation from the mean of color channels at the same spatial position. Brightness feature maps are extracted for each color channel of each color balanced version of the input image given in Eqn. (4) as

$$B_{I_*} = |I_* - M| \tag{4}$$

where B_{I_*} is the brightness map of the color channel I_* and M denotes the average of R, G and B channels at each pixel location.

Since the brightness is not well-preserved in underwater images, this study enhances the brightness map in order to highlight pixels which are not sufficiently saturated. To do so, channel-based brightness histograms are normalized to approximate the corresponding probability mass function. Then, cumulative mass function is calculated, denormalized and inverted to be used as a transfer function for enhancement.

Laplacian Contrast. The Laplacian contrast feature measures the detail information in an image. It assigns higher values to edges and fine textured areas. A simple Laplacian sharpening kernel is used to calculate this feature map, denoted as L_{I_*},

for all color channels of each color balanced image. Absolute values are processed.

C. Multi-scale Fusion and Post-processing

After all feature maps are characterized for each color channel, they are multiplied to generate a refined weight map for each color balanced version of the input image given in Eqn. (5) as

$$W_{I_*} = P_{I_*} \times E_{I_*} \times S_{I_*} \times B_{I_*} \times L_{I_*} \tag{5}$$

where W_{I_*} represents final weights for each color channel R, G and B per color balance. All these maps are first linearly normalized to the range $[0, 1]$ and then normalized to be sum-to-one at each spatial position.

The well-known multi-scale fusion [11], [18] mechanism is adapted with the Laplacian pyramid $\mathcal{L}$ to decompose each color balanced input images in to ℓ-levels of distinct resolutions, and the Gaussian pyramid $\mathcal{G}$ to accomplish the same operation for the corresponding final feature maps. The fusion is applied at each level of the pyramidal decomposition and a fused Laplacian pyramid is obtained given in Eqn. (6) as

$$\mathcal{L}(F^\ell) = \sum_{k=1}^{3} \mathcal{G}\{W_k^\ell\}\mathcal{L}\{C_k^\ell\} \tag{6}$$

where W_k and C_k represent 3-channel final weight maps and the corresponding color balanced images, respectively. The fused decomposition $\mathcal{L}(F^\ell)$ is later used to obtain the output image ($\ell = 5$).

The final dehazed output is obtained with the new red-channel from above fusion, and green and blue channels of white balanced image, which is followed by gamma correction to further enhance the contrast ($\gamma = 1.25$).

III. EXPERIMENTAL RESULTS

The underwater image dehazing algorithm is compared with eight competing methods from literature through three statistical metrics generally used in this research domain. Five different images from the U45 Underwater Test Dataset [7], namely Image 1, Image 2, Image 3, Image 4 and Image 5 (labeled as ORG), are tested as illustrated in the first column of Fig. 2.

The statistical evaluation metrics are: (*i*) underwater image quality measure (UIQM) [19], (*ii*) underwater color image quality evaluation (UCIQE) [20] and patch-structure contrast quality index (PCQI) [21]. UIQM is a non-reference quality metric that measures colorfulness, sharpness and contrast in an image. UCIQE is also another non-reference metric for underwater images. It measures the contrast, chroma and saturation values in CIELab color space, to specify the image quality. In addition, PCQI is one of the common –with reference– quality index which is based on image contrast assessment. It evaluates a local patch structure to calculate the contrast enhancement. For the all three image quality indexes, the higher metric value presents that the image has a better visual quality.
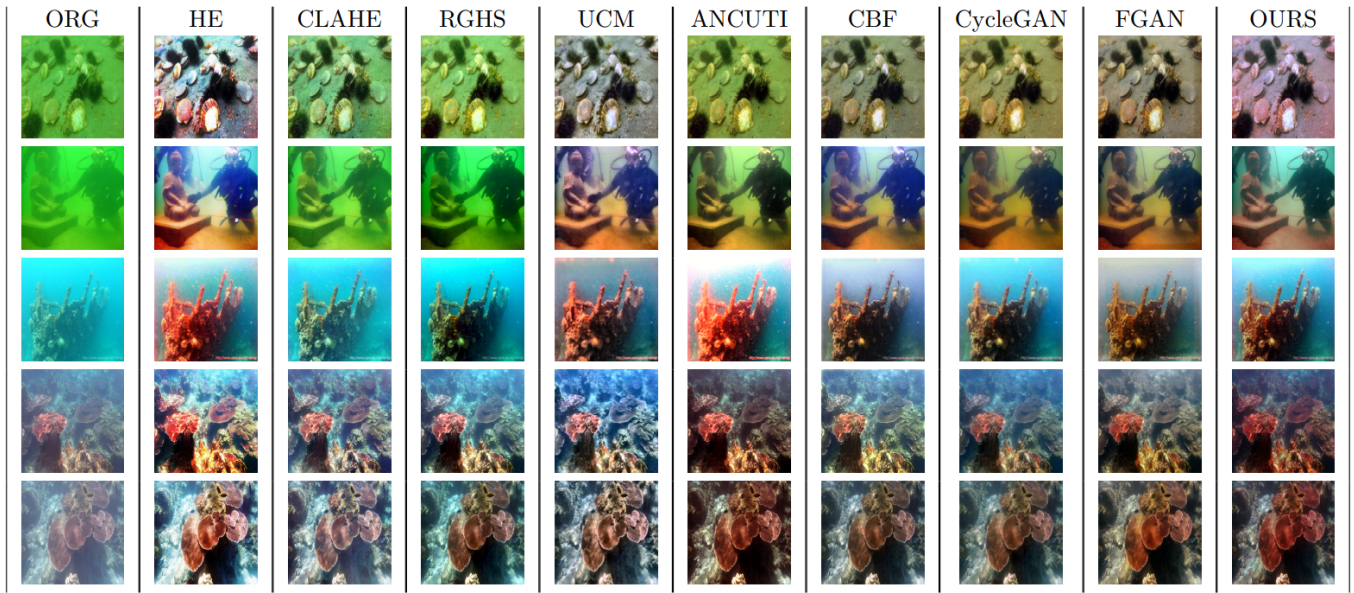
Fig. 2. (Left-to-right) Input image, and the output images of HE [3], CLAHE [4], RGHS [5], UCM [6], Ancuti [7], Ancuti (CBF) [8], CycleGAN [9], FGAN [10] and OURS.

TABLE I
STATISTICAL SCORES FOR TEST IMAGES. THE HIGHEST SCORES ARE IN BOLDFACE

	ORG			HE [3]			CLAHE [4]			RGHS [5]			UCM [6]		
	UIQM	UCIQE	PCQI	UIQM	UCIQE	PCQI	UIQM	UCIQE	PCQI	UIQM	UCIQE	PCQI	UIQM	UCIQE	PCQI
Image 1	2,2186	0,4610	-	5,2201	0,6420	1,0248	3,7257	0,5487	0,5487	3,2988	0,5815	0,8599	4,0633	0,5696	0,8641
Image 2	0,0086	0,3954	-	4,6790	0,7050	0,7970	2,0538	0,4907	0,7151	0,8523	0,5888	0,7590	4,3897	0,6427	0,8306
Image 3	-0,5288	0,4368	-	4,5219	0,7053	0,7351	1,2173	0,5402	0,6818	0,6649	0,6497	0,6702	4,5861	0,7163	0,7069
Image 4	4,1743	0,5043	-	5,2039	0,7049	0,9559	5,1211	0,5952	0,9625	4,3667	0,6646	0,9092	**6,0058**	0,6327	0,8738
Image 5	4,2262	0,4670	-	5,3778	0,6799	0,9172	5,3918	0,5712	0,9166	5,0778	0,6633	0,9571	6,1476	0,6512	0,9178
avg	2,0198	0,4529	-	5,0005	0,6874	0,8860	3,5019	0,5492	0,7649	2,8521	0,6296	0,8311	5,0385	0,6425	0,8386
std	2,0045	0,0360	-	**0,3360**	**0,0247**	0,1057	1,6468	0,0349	0,1537	1,8017	0,0367	0,1038	0,8651	0,0468	0,0715

	ANCUTI [7]			ANCUTI (CBF) [8]			CycleGAN [9]			FGAN [10]			OURS		
	UIQM	UCIQE	PCQI	UIQM	UCIQE	PCQI	UIQM	UCIQE	PCQI	UIQM	UCIQE	PCQI	UIQM	UCIQE	PCQI
Image 1	5,0110	0,5648	**1,2142**	5,0089	**2,2063**	0,0876	4,8550	0,5672	0,7931	5,0544	0,5713	0,9819	**5,6351**	0,5818	1,1983
Image 2	**5,5520**	0,6407	**1,1704**	4,7228	**6,3399**	0,2273	4,7941	0,6177	0,2073	4,9139	0,6354	0,9735	4,0528	0,6471	1,1104
Image 3	**4,6909**	0,6342	1,0576	4,5542	**11,8285**	0,1779	2,8075	0,6614	0,1705	4,4479	0,6080	0,8891	3,5401	0,6858	**1,0763**
Image 4	4,6071	0,6296	**1,2635**	5,2990	**5,0517**	0,0964	4,4679	0,5884	0,1357	5,2048	0,5949	0,9119	5,8667	0,5979	0,9226
Image 5	5,5494	0,6217	**1,2143**	5,4705	**4,6064**	0,1017	5,2911	0,6006	0,1247	5,9081	0,6251	0,8233	**6,2430**	0,6294	0,9126
avg	5,0821	0,6182	**1,1840**	5,0111	**6,0066**	0,1382	4,4431	0,6071	0,2863	**5,1058**	0,6069	0,9159	5,0675	0,6284	1,0440
std	0,4057	0,0274	0,0697	0,3423	3,2038	**0,0551**	0,8588	0,0318	0,2551	0,4745	0,0226	0,0583	1,0682	0,0367	0,1107

Competing methods include HE [3], CLAHE [4], RGHS [5], UCM [6], Ancuti [7], Ancuti (CBF) [8], CycleGAN [9], FGAN [10]. All these algorithms are executed with their default parameter values under Matlab and Python environments. The visual results of all methods are illustrated in Fig. 2 in which a side-by-side visual comparison indicates that the proposed method generates visually realistic and more appealing outcomes. In addition, the obtained statistical metric scores are given in Table I. It can be clearly concluded that the proposed underwater image enhancement method produces highly competitive results and surpasses most of the competing approaches on average.

IV. CONCLUSION

This paper develops an underwater image dehazing algorithm which combines several techniques. The red-channel of the input image is recovered with the help of PCA, well-exposedness, saliency, brightness and Laplacian contrast feature maps through a multi-scale fusion of different color balanced versions of the input image. Experimental results prove the effectiveness of the proposed algorithm both visually and statistically.

534

<center>REFERENCES</center>

[1] A. AbuNaser, I. A. Doush, N. Mansour, and S. Alshattnawi, "Underwater image enhancement using particle swarm optimization," *J. Intell. Syst.*, vol. 24, no. 1, pp. 99–115, 2015.

[2] R. Schettini and S. Corchs, "Underwater image processing: State of the art of restoration and image enhancement methods," *EURASIP J. Adv. Signal Process.*, vol. 2010, no. 1, 2010.

[3] K. He, J. Sun, and X. Tang, "Single image haze removal using dark channel prior," *IEEE Trans. Patt. Anal. Mach. Intell.*, vol. 33, no. 12, pp. 2341–2353, 2011.

[4] G. Yadav, S. Maheshwari, and A. Agarwal, "Contrast limited adaptive histogram equalization based enhancement for real time video system," in *Int. Conf. Adv. Comput. Commun. Info.*, 2014, pp. 2392–2397.

[5] D. Huang, Y. Wang, W. Song, J. Sequeira, and S. Mavromatis, "Shallow-water image enhancement using relative global histogram stretching based on adaptive parameter acquisition," in *Int. Conf. MultiMed. Model.*, 2018, pp. 453–465.

[6] K. Iqbal, M. Odetayo, A. James, R. A. Salam, and A. Z. H. Talib, "Enhancing the low quality images using unsupervised colour correction method," in *IEEE Int. Conf. Syst. Man Cyber.*, 2010, pp. 1703–1709.

[7] C. Ancuti, C. O. Ancuti, T. Haber, and P. Bekaert, "Enhancing underwater images and videos by fusion," in *IEEE Conf. Comp. Vis. Patt. Recog.*, 2012, pp. 81–88.

[8] C. O. Ancuti, C. Ancuti, C. De Vleeschouwer, and P. Bekaert, "Color balance and fusion for underwater image enhancement," *IEEE Trans. Image Process.*, vol. 27, no. 1, pp. 379–393, 2018.

[9] J. Park, D. K. Han, and H. Ko, "Adaptive weighted multi-discriminator CycleGAN for underwater image enhancement," *J. Marine Sci. Eng.*, vol. 7, no. 7, 2019.

[10] H. Li, J. Li, and W. Wang, "A fusion adversarial underwater image enhancement network with a public test dataset," https://arxiv.org/abs/1906.06819, 2019.

[11] T. Mertens, J. Kautz, and F. Van Reeth, "Exposure fusion: A simple and practical alternative to high dynamic range photography," *Comput. Graph. Forum*, vol. 28, no. 1, pp. 161–171, 2009.

[12] D. Karakaya, O. Ulucan, and M. Turkan, "PAS-MEF: Multi-exposure image fusion based on principal component analysis, adaptive well-exposedness and saliency map," in *IEEE Int. Conf. Acous. Speech Signal Process.*, 2022, pp. 2345–2349.

[13] X. Hou, J. Harel, and C. Koch, "Image signature: Highlighting sparse salient regions," *IEEE Trans. Pattern Anal. Mach. Intell.*, vol. 34, no. 1, pp. 194–201, 2012.

[14] M. Kumar and A. K. Bhandari, "Contrast enhancement using novel white balancing parameter optimization for perceptually invisible images," *IEEE Trans. Image Process.*, vol. 29, pp. 7525–7536, 2020.

[15] X. Li and J. Wu, "Improved gray world algorithm based on salient detection," *Commun. Comp. Inf. Sci.*, pp. 315–321, 2013.

[16] D. Marini, A. Rizzi, and C. Carati, "Color constancy effects measurement of the retinex theory," in *SPIE*, vol. 3648, 1998, pp. 249–256.

[17] Y. Tao, L. Dong, and W. Xu, "A novel two-step strategy based on white-balancing and fusion for underwater image enhancement," *IEEE Access*, vol. 8, pp. 217 651–217 670, 2020.

[18] P. J. Burt and R. J. Kolczynski, "Enhanced image capture through fusion," in *IEEE Int. Conf. Comput. Vis.*, 1993, pp. 173–182.

[19] K. Panetta and C. Gao, "Human-visual-system-inspired underwater image quality measures," *IEEE J. Oceanic Eng.*, vol. 41, pp. 1–11, 10 2015.

[20] M. Yang and A. Sowmya, "An underwater color image quality evaluation metric," *IEEE Trans. Image Process.*, vol. 24, no. 12, pp. 6062–6071, 2015.

[21] S. Wang, K. Ma, H. Yeganeh, Z. Wang, and W. Lin, "A patch-structure representation method for quality assessment of contrast changed images," *IEEE Signal Process. Lett.*, vol. 22, pp. 2387–2390, 12 2015.

<center>535</center>